Fractional behavior in multidimensional Hamiltonian systems describing reactions

Akira Shojiguchi,[1,*] Chun-Biu Li,[2,†] Tamiki Komatsuzaki,[2,†] and Mikito Toda[1]
[1]*Physics Department, Nara Women's University, Kita-Uoya-Nishimachi, Nara 630-8506, Japan*
[2]*Nonlinear Science Laboratory, Department of Earth and Planetary Sciences, Faculty of Science, Kobe University, Nada, Kobe 657-8501, Japan*
(Received 9 July 2007; published 8 November 2007)

The fractional behavior is presented for a minimal Hamiltonian system of three degrees of freedom which describes reaction processes. The model has a double-well potential where the Arnold web within the well is nonuniform. The survival probability within the well exhibits power law decay in addition to exponential decay. Moreover, the trajectories of the power law decay exhibit $1/f$ spectra and subdiffusion in the action space, while the trajectories of the exponential decay show Lorentzian spectra and normal diffusion. Transient features of these statistical properties reveal the dynamical connection, i.e., how trajectories approach to (depart from) the Arnold web from (to) the region around the potential saddle. In particular, a wavelet analysis enables us to extract transient features of the resonances. Based on these results, we suggest that resonance junctions including higher-order resonances are important for understanding the dynamical origins of the fractional behavior in reaction processes.

DOI: 10.1103/PhysRevE.76.056205 PACS number(s): 05.45.−a, 34.10.+x, 82.20.Db

I. INTRODUCTION

Fractional behavior in Hamiltonian chaos is of interest for a variety of systems ranging from billiards to water clusters [1–6]. In these studies, unconventional statistical features have been found, such as anomalous diffusion, time correlation with an algebraic decay, and $1/f$ spectra. For systems of two degrees of freedom (2DOF), the dynamical origin of the fractional behavior is well understood, based on the hierarchical structures formed by resonant tori [1]. There, tori constitute dynamical barriers for transport: The two-dimensional tori are impenetrable boundaries, thereby dividing the three-dimensional equienergy surface into separate regions. On the contrary, for systems of more than 2DOF, the origins of the fractional behavior are not understood yet: The mechanism for systems of 2DOF is not relevant here since the dimension of the tori is not sufficient to block transport in the phase space. Therefore, understanding the dynamical origins of fractional behavior for systems of more than 2DOF presents a new problem in nonlinear physics.

In particular, the existence of fractional behavior in Hamiltonian systems raises a serious question for the foundation of statistical reaction theory. In the conventional theory, reaction processes are supposed to be normal diffusive motions [7]. This idea is based on the assumption that the characteristic time scale for the reaction is much longer than that for trajectories to lose their memories. Thus, reaction processes are regarded as being composed of many erratic dynamical motions, leading to the Brownian type of diffusion. However, recent studies on reaction processes cast doubt on this assumption. For example, $1/f$ spectra are found in simulations of water clusters [3,4], and power law decays are observed in correlations of vibrational dephasing [8,9]. These studies indicate that the basic assumption of the statistical reaction theory should be reexamined by taking into account the existence of the fractional behavior.

In order to reveal the foundation and limitations of statistical reaction theory, the study of Hamiltonian systems of more than 2DOF is necessary. In particular, Hamiltonians describing reaction processes have potential minima and saddles. Minima correspond to stable configurations of molecules, and saddles correspond to configurations which link stable ones. For each minimum and saddle, the normal form theory provides us with a method to understand the dynamics around them. However, local analysis is not sufficient for understanding the reaction processes. We need to take into account global aspects of the system, that is, dynamics near saddles and around minima, and how they are connected [10,11].

Around minima, the normal form theory offers a method to represent the Hamiltonian in terms of nonlinear vibrational modes [12]. The normal form breaks down at locations in the phase space where nonlinear resonance takes place, and enhanced energy transfer occurs among these vibrational modes. In general, nonlinear resonances constitute a network in the action space called the Arnold web, and resonance overlap causes global chaos [13]. Thus, the characteristics of the Arnold web are important to understand the mechanism of intramolecular vibrational-energy redistribution (IVR) [14–16]. In particular, nonuniformity of the Arnold web and distribution of resonance overlaps is crucial for revealing the mechanism of fractional behavior, as we will show in this paper.

Around saddles, the normal form theory has been recently developed based on geometric structures in the phase space called normally hyperbolic invariant manifolds (NHIMs) [17–19]. The theory offers a sound foundation for the concept of transition states (TSs), i.e., the key concept in the dynamical reaction theory for systems of many DOF. It is

*Present address: System Jisso Research Laboratories, NEC Corporation, 1120 Shimokuzawa, Sagamihara, Kanagawa 229–1198, Japan. a-shoujiguchi@ap.jp.nec.com
†Present address: Research Institute for Electronic Science, Hokkaido University, Kita 12 Nishi 6, Kita-Ku, Sapporo 060–0812, Japan

shown that the theory can be applied to those reactions with a moderate energy above the saddle [20]. The theory has been applied to a wide range of reactions involving rearrangements of particles in the fields of atomic, molecular [18,21,22], and cluster physics [23,24], and even in celestial mechanics [25].

As for the connection between the NHIM around the saddle and the Arnold web in the well, no analytical methods are available at present. This is the most challenging part of this problem. In order to understand the connection, we need to analyze the heteroclinic intersections between the stable (unstable) manifolds of the NHIM around the saddle and the unstable (stable) manifolds emanating from the Arnold web. There exist a few studies which reveal hyperbolic structures in the web such as whiskered tori and unstable periodic orbits (POs) [26–30]. However, no study has been done to reveal the dynamical connection between these hyperbolic structures in the Arnold web and the NHIM around the saddle.

In this paper, we present a numerical manifestation of fractional behavior for a minimal Hamiltonian system of 3DOF describing nonergodic reaction processes. Fractional behavior is revealed in the survival probability, Fourier spectra of autocorrelation functions, and diffusive properties of motions. The transient features of these statistical properties reveal how the trajectories starting near the NHIM arrive at, wander around in, and depart from the web. In particular, a wavelet analysis enables us to extract transient features of resonances including higher-order resonances. Based on these results, we present a conjecture concerning the dynamical origins of the fractional behavior in reactions.

The content of this paper is the following. In Sec. II, we give a brief explanation of the key concepts in dynamical reaction theory, i.e., the Arnold web and the NHIM around the saddle. In Sec. III, we introduce a minimal Hamiltonian model describing nonergodic reaction processes, i.e., a system of 3DOF with a nonuniform Arnold web in the well. In Sec. IV, we show that the survival probability in the potential well exhibits power law decay in addition to exponential decay. We also indicate that the coexistence of these decays results from the nonuniformity of the Arnold web. In Sec. V, we show the differences in statistical properties, i.e., the Fourier spectra and the diffusivity, between the trajectories of power law decay and those of exponential decay. In Sec. VI, we demonstrate that transient features of the statistical quantities reveal the dynamical connection between the NHIM around the saddle and the Arnold web in the well. In Sec. VII, the wavelet analysis is applied to investigate transient features of the resonant behavior, including higher-order resonances. Here, we suggest the importance of hierarchical structures of resonance junctions including higher-order resonances. In Sec. VIII, we study how the coexistence of the power law and exponential decays persists as we change the energy or the parameters of the system. In Sec. IX, we summarize our results and point out future problems concerning the dynamical origins of the fractional behavior in reactions.

II. DYNAMICAL REACTION THEORY

In this section, we briefly explain the basic concepts of dynamical reaction theory, i.e., the Arnold web and the NHIM around the saddle. These concepts play a crucial role in understanding the reaction processes from a standpoint beyond the conventional statistical theory.

A. Arnold web

The Arnold web offers a clue to understand statistical features of the dynamics in the potential well.

Suppose that the minimum of the potential is located at $(q_1,\ldots,q_N)=(0,\ldots,0)$. Then, the Hamiltonian of N DOF is expanded around the minimum as follows:

$$H=\sum_{j=1}^{N}\left(\frac{p_j^2}{2}+\frac{\omega_j^2 q_j^2}{2}\right)+\sum_{n=3}^{\infty}H_n, \tag{1}$$

where ω_j for $j\geqslant 1$ are real, and H_n consists of the terms of nth degree in $(\mathbf{q},\mathbf{p})=(q_1,\ldots,q_N,p_1,\ldots,p_N)$. Given the Hamiltonian Eq. (1), we try to eliminate as many coupling terms as possible by canonically transforming the original coordinates and momenta to new ones. If we succeed in eliminating all of them, the system is integrable and no processes of energy exchange take place among the modes represented by the new coordinates and momenta. However, such transformations do not exist in general because of nonlinear resonances [12]. This is the problem of small denominators.

Nonlinear resonances generally constitute a network in the action space called the Arnold web. When these resonances do not overlap with each other, a motion called "Arnold diffusion" takes place along the resonance lines [31,32]. However, the characteristic time scale of Arnold diffusion is very long compared to the periods of the vibrational modes [33]. On the other hand, when resonances overlap, global chaos occurs [13], and the dynamics across the resonances is more "visible" [34,35]. In particular, the resonance junctions, i.e., the intersections of resonances, play an important role for the dynamics on the Arnold web [26–29,34,35]. For Hamiltonian systems of N DOF, the number of independent resonances that intersect ranges from 2 to $N-1$, and the hierarchy of these intersections is characterized by the Hasse diagram [36] (see [37] for an explanation of the Hasse diagram). Moreover, the hierarchical ordering of POs was recently found for near-integrable systems of 3 DOF [30]. They argue that this ordering reflects the hierarchy of resonant tori in an integrable limiting case. However, no studies have been done to investigate whether such hierarchical structures in Hamiltonian systems of more than two DOF give rise to anomalous features in their statistical behavior. Thus, characteristics of the Arnold web, such as whether the Arnold web is uniform or not and how the resonance junctions are distributed, play an important role in the statistical features of the dynamics in the well.

B. Normally hyperbolic invariant manifolds

We start our explanation of NHIMs with the simplest case, i.e., the NHIM around a saddle of index 1. Suppose that a Hamiltonian of N degrees of freedom is expanded around a saddle located at $(q_1,\ldots,q_N)=(0,\ldots,0)$ as follows:

$$H = \left(\frac{p_1^2}{2} - \frac{\mu_1^2 q_1^2}{2}\right) + \sum_{j=2}^{N}\left(\frac{p_j^2}{2} + \frac{\omega_j^2 q_j^2}{2}\right) + \sum_{n=3}^{\infty} H_n, \qquad (2)$$

where μ_1 and ω_j for $j \geqslant 2$ are real, and H_n consists of terms of nth order in $(\mathbf{q},\mathbf{p})=(q_1,\ldots,q_N,p_1,\ldots,p_N)$. Then, the coordinate q_1 lies, locally near the saddle, along the direction of the eigenvector corresponding to the negative eigenvalue of the Hessian matrix at the saddle.

In eliminating the coupling terms between (q_1,p_1) and the rest of the degrees of freedom, the problem of small denominators does not exist. It is because no resonance takes place between the "imaginary frequency" $i\mu_1$ and the real frequencies $\omega_j (j \geqslant 2)$. Thus, all of the coupling terms involving (q_1,p_1) can be eliminated by the canonical transformation. Then, the degree of freedom (q_1',p_1') transformed from (q_1,p_1) becomes decoupled from the rest of the degrees of freedom at least locally around the saddle. This means that the manifold M defined by $q_1'=0$ and $p_1'=0$ is invariant under the dynamics. Moreover, the normal directions to the manifold M are hyperbolic, i.e., the trajectories approach or leave the manifold M along these directions. We call the manifold M the NHIM around the saddle.

In the context of reaction theory, the space defined by $q_1'=0$ gives the dividing hypersurface between the reactant and the product. This is the TS in the mathematically rigorous sense. The TS thus defined is free from the so-called recrossing problem. Thus, the normal form theory based on the NHIM provides a mathematically sound definition of the concept of TSs. Moreover, the stable (unstable) manifolds of the NHIM define the reaction conduit through which all the reactive trajectories pass from the reactant to the product, or vice versa. Therefore, these manifolds offer a crucial clue to understanding the controllability of the reaction, and to investigate dynamical correlation in reaction processes taking place over multiple saddles.

In general, a NHIM is a manifold where instability in either a forward or a backward direction of time along its normal directions is much stronger than that along its tangential directions [38–40]. NHIMs are structurally stable under perturbations. The wider the gap of instability between the normal directions and the tangential ones, the more structurally stable is the NHIM. Using the Lyapunov exponents, we can define a NHIM as a manifold where the absolute values of the Lyapunov exponents along its normal directions are much larger than those along its tangential directions. Thus, we can define the NHIM even when the degrees of freedom along the tangential directions are also hyperbolic, as long as the absolute values of their Lyapunov exponents are smaller than those along the normal directions [20].

III. MODEL HAMILTONIAN

In this section, we introduce a minimal Hamiltonian system of 3DOF describing reaction processes with nonergodic dynamics in the well. The model has a double-well potential where the Arnold web within the well is nonuniform. The processes of going over the potential saddle are regarded as isomerization, where the molecule changes its configuration:

$$H = H_0 + H_1,$$

$$H_0 = \frac{p_1^2}{2} - \frac{\lambda^2 q_1^2}{2} + b q_1^4 + \sum_{i=2}^{3}\left(\frac{p_i^2}{2} + \frac{\omega_i^2 q_i^2}{2} + b q_i^4\right),$$

$$H_1 = e^{-(q_1-1)^2/\sigma^2}[a_1 q_2^2 q_3^2 + a_2 (q_1-1)^2 (q_2^2+q_3^2)]. \qquad (3)$$

Here q_1 is the reaction coordinate, and q_i $(i=2,3)$ are the bath coordinates. The values of the frequencies are $\omega_1=1.02$, $\omega_2=0.94$, and $\omega_3=1.04$. The frequency $\omega_1=\lambda/\sqrt{2}$ is the unperturbed frequency at the bottom of the well at $q_1=1$. We choose the coupling function and the parameters ($\sigma=0.5$, $a_1=0.1$, $a_2=0.9$, and $b=0.5$) so that the interactions among the modes take place more in the well than near the saddle. This is valid for energy values slightly above the saddle energy [23].

In the following, we estimate approximate locations of the primary resonances in the action space using the unperturbed part of the Hamiltonian.

The unperturbed Hamiltonians of the bath coordinates $h_i = p_i^2/2 + \omega_i^2 q_i^2/2 + b q_i^4$ $(i=2,3)$ are nonlinear oscillators. They are integrable with the following constants of motion:

$$J_i(h_i) = \frac{1}{2\pi}\oint dq_i p_i(q_i) = \frac{A}{3k^2}[(2k_i^2-1)E(k_i) + (1-k_i^2)K(k_i)], \qquad (4)$$

where $k_i^2 = \alpha_i^2/(\alpha_i^2+\beta_i^2)$, $\alpha_i^2 = (-\omega_i^2 + \sqrt{\omega_i^4 + 16bh_i})/4b$, $\beta_i^2 = (\omega_i^2 + \sqrt{\omega_i^4+16bh})/4b$, and $A_i = (2\alpha_i^2/\pi)\sqrt{2b(\alpha_i^2+\beta_i^2)}$. Here, the elliptic functions are defined as $E(k) = \int_0^{\pi/2} d\phi \sqrt{1-k^2\sin^2\phi}$ and $K(k) = \int_0^{\pi/2} d\phi (1/\sqrt{1-k^2\sin^2\phi})$. By transforming the Hamiltonian of Eq. (3) at the bottom of the well, we obtain the nonlinear frequencies for the bath coordinates up to the first order of the action variables,

$$\bar{\omega}_i(J_i) = \frac{\partial H_0}{\partial J_i} = \omega_i + \frac{3b}{\omega_i^2} J_i + O(J_i^2) \quad (i=2,3), \qquad (5)$$

where we use the action variables of Eq. (4).

The reaction coordinate has the action variable in the well

$$J_1(h_1) = \frac{\sqrt{2}\lambda}{3\pi}(\alpha_1+\beta_1)[E(k_1) - \alpha_1\beta_1 K(k_1)], \qquad (6)$$

where the unperturbed Hamiltonian of the reaction coordinate is expressed as $h_1 = p_1^2/2 - \lambda^2 q_1^2/2 + b q_1^4$ for the range $-\lambda^2/4 < h_1 < 0$. Here, we use the notations $\alpha_1 = \sqrt{1-\sqrt{1+4h_1/\lambda^2}}$, $\beta_1 = \sqrt{1+\sqrt{1+4h_1/\lambda^2}}$, and $k_1 = (\beta_1 - \alpha_1)/(\beta_1+\alpha_1)$. The nonlinear frequency of the reaction coordinate in the well is given, up to the first order of the action variable (6), by

$$\bar{\omega}_1 = \frac{\partial H_0}{\partial J_1} = \omega_1 - \frac{3}{4} J_1 + O(J_1^2). \qquad (7)$$

Then, we can estimate that the system has primary resonances given by

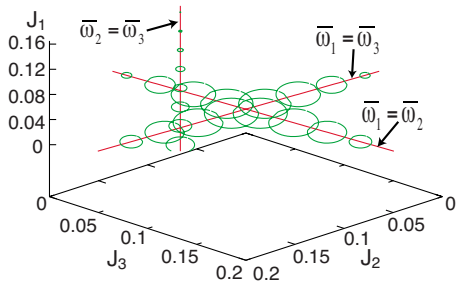

FIG. 1. (Color online) Arnold web of the primary resonances. The radii of the circles indicate their widths.

$$\bar{\omega}_1 = \bar{\omega}_2, \quad \bar{\omega}_1 = \bar{\omega}_3, \quad \bar{\omega}_2 = \bar{\omega}_3. \tag{8}$$

In Fig. 1, we show these resonances of Eq. (8) in the action space by estimating their locations approximately using the unperturbed Hamiltonian. There, we also indicate the widths of the resonances by the radii of the circles. We notice that, in Fig. 1, the Arnold web of the primary resonances is sparse. On the other hand, there exist three intersections where two resonances meet, i.e., resonance junctions. Near these three junctions, the regions of the primary resonances overlap with each other. Then, global chaos exist there based on the criterion of overlapping resonance. Thus, chaos is weak in some parts of the Arnold web and strong in other parts. Therefore, the Arnold web of the system is nonuniform. These features will play an important role in the following results.

The NHIM and its stable (unstable) manifolds are constructed near the saddle by eliminating the coupling terms between the reaction coordinate and the bath coordinates. In the following, the initial conditions are chosen to be uniformly distributed on the unstable manifold of the NHIM near the saddle. The energy E of these initial conditions is set to be $E=0.1$ except in Sec. VIII. Note that the potential energy at the saddle and the minimum is 0 and -0.125, respectively. By numerically calculating the trajectories from these initial conditions, we can extend the unstable manifold of the NHIM from near the saddle to the potential well.

IV. FRACTIONAL BEHAVIOR IN SURVIVAL PROBABILITY

In this section, we present fractional behavior in the survival probability. The survival probability is calculated as a function of the residence time t_r. The residence time t_r inside the well is estimated for each trajectory in units of the period $t_1=2\pi\omega_1$. By adding the number of trajectories with their residence times from t_r to infinity, we obtain the number of trajectories that remain in the well at the residence time t_r. The ratio of this quantity to the total number of trajectories gives the survival probability. We also estimate the survival probability as a function of the crossing number n. The crossing number for each trajectory is estimated as follows. We count the number of crossings each time the trajectory crosses a surface of section ($q_1=1$ with $p_1>0$) until the trajectory leaves the well. The total number of crossings for the trajectory is its crossing number n. We estimate the survival probability as a function of the crossing number n in the same way as we do for the residence time t_r.

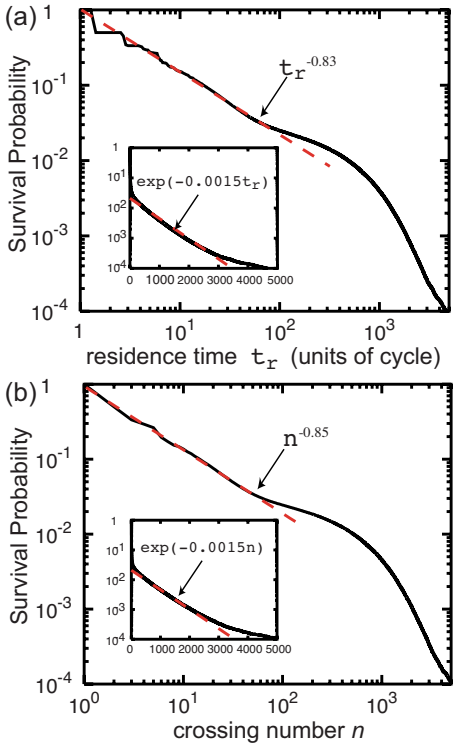

FIG. 2. (Color online) Survival probabilities shown by log-log plots (a) as a function of the residence time t_r and (b) as a function of the crossing number n (solid lines), with fittings $t_r^{-\gamma}$ and $n^{-\gamma}$ (dashed lines), respectively. The insets show log-linear plots (solid lines) with fittings $\exp(-\alpha t_r)$ and $\exp(-\alpha n)$, respectively (dashed lines).

In Fig. 2, the survival probabilities are shown as a function of the residence time t_r and of the crossing number n. In both of the figures, the survival probabilities reveal two distinct time scales. For the survival probability $P(t_r)$ as a function of the residence time t_r, $P(t_r)$ decays as $t_r^{-\gamma}$ up to about 100 cycles, and, for longer time scales, $P(t_r)$ decays as $\exp(-\alpha t_r)$. By fitting the function $P(t_r)$, we obtain $\gamma=0.82$ and $\alpha=0.0015$. We also see a similar behavior for the survival probability as a function of the crossing number n.

Now we investigate the origin of the existence of the two time scales based on the nonuniformity of the Arnold web. In Fig. 3(a), the average locations in the action space (J_2,J_3,J_1) are plotted for trajectories exhibiting power law decay. The location of the trajectory is recorded each time it crosses a surface of section ($q_1=1$ with $p_1>0$). After that, all the recorded locations are averaged over its residence time. There, a typical example of the trajectories is also shown. In Fig. 3(b), the average locations in the action space (J_2,J_3,J_1) are plotted for trajectories exhibiting exponential decay with a typical example of the trajectories. In Fig. 3, the locations of the primary resonances are indicated for comparison.

Comparing Figs. 3(a) and 3(b), we can see that the average locations are distributed in different regions in the action space. This suggests that there exist dynamical structures which prevent the trajectories from exploring the whole

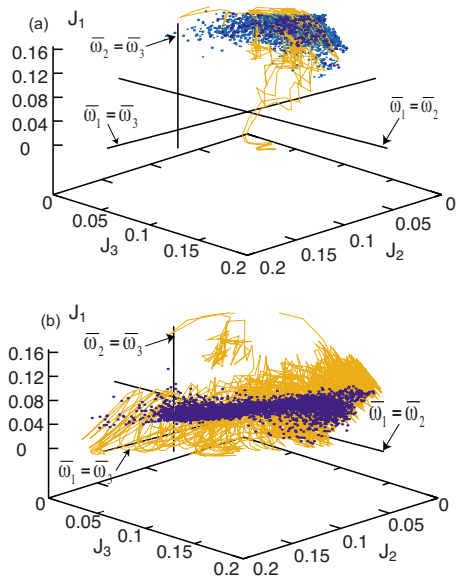

FIG. 3. (Color online) Blue (dark gray) points show the average locations in the action space (a) for the trajectories exhibiting power law decay, and (b) for the trajectories exhibiting exponential decay. The orange (gray) curves denote typical trajectories in the action space exhibiting (a) the power law and (b) the exponential decay, respectively.

phase space. In particular, while the locations of the trajectories for the exponential decay are spread around the resonance junctions, the locations of the trajectories for the power law decay lie apart from the resonance junctions. Therefore, while the trajectories of the exponential decay experience fully chaotic regions, the trajectories of the power law decay do not penetrate into these regions. Thus, the coexistence of the two time scales in the survival probability results from the coexistence of regions with different dynamical properties.

We indicate more quantitatively how the coexistence of the two time scales is related to the nonuniformity of the Arnold web. In Fig. 4, we draw the averaged distances of the trajectories from the resonance lines in the action space as functions of the crossing number n. The distance is estimated each time the trajectory crosses a surface of section ($q_1=1$ with $p_1>0$), and these values are averaged until the trajectory leaves the well. The average is further taken over trajectories that have the same crossing number n. Thus, we obtain the distance as a function of the crossing number. There, we show the averaged distance d_1 from the resonance line $\bar{\omega}_1=\bar{\omega}_2$, and the averaged distance d_2 from the resonance line $\bar{\omega}_1=\bar{\omega}_3$, respectively. Note that both of the resonances involve the reaction coordinate, thereby contributing to the processes of energy exchange involving the reaction coordinate.

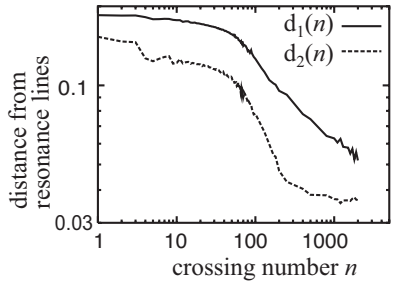

FIG. 4. Averaged distances from the two resonance lines as functions of the crossing number n shown as a log-log plot. The solid (dashed) line indicates the distance $d_1(n)$ [$d_2(n)$] from the resonance line with $\bar{\omega}_1=\bar{\omega}_2$ ($\bar{\omega}_1=\bar{\omega}_3$).

We can see that the distances decrease as the crossing number n increases. This means that, the closer to the resonances the trajectories wander, the longer they stay in the well. In particular, both of the distances have smaller values for the trajectories with larger crossing numbers. This indicates that the trajectories with larger values of the crossing number wander near the resonance junctions. Moreover, both of values of the distances d_1 and d_2 drop around $n=100$. The value of the crossing number $n=100$ coincides with the boundary between the power law and exponential decays of the survival probability in Fig. 2(b). Thus, the coexistence of the two time scales in the survival probability results from the coexistence of the two regions in the Arnold web: One is remote from the resonance junctions and the other near the junctions.

V. ANOMALOUS DIFFUSION IN ACTION SPACE

In this section, we demonstrate the difference in statistical features between the trajectories of the power law and the exponential decays.

In Fig. 5, we display Fourier spectra of the time correlation of the action J_1 for a trajectory of the power law decay and one of the exponential decay, respectively. Fittings by $1/\omega$ and $a/(\omega^2+b)$ are also shown there. We see that, while the Fourier spectrum for a trajectory of the power law decay reveals a $1/f$ behavior, the Fourier spectrum for a trajectory of the exponential decay reveals a Lorentzian behavior. Other trajectories of the power law decay and those of the exponential decay exhibit the same features, respectively. This indicates that, while the trajectories of the power law decay have long-lasting memories, the trajectories of the exponential decay do not.

Diffusion in the action space also exhibits the corresponding difference between the trajectories of the power law and of the exponential decays. We define local diffusivity in the action space by

$$\sigma_k(t,t_0)=\langle[J_k(t)-J_k(t_0)]^2\rangle, \tag{9}$$

where the square displacement of J_k during the time interval between t_0 and t is averaged over an ensemble of the trajectories within a range of the exponential decay. By changing the time t_0, we can estimate diffusivity locally in time.

In Fig. 6(a), the diffusivity $\sigma_1(t,t_0)$ is shown for an ensemble of trajectories whose residence times t_r are in the range of the power law decay, i.e., $90<t_r<100$. We can see that the trajectories exhibit subdiffusion of $(t-t_0)^p$ with $p=0.53$. On the other hand, in Fig. 6(b), the diffusivity $\sigma_1(t,t_0)$ is shown for an ensemble of trajectories whose residence times t_r are in the range of the exponential decay, i.e.,

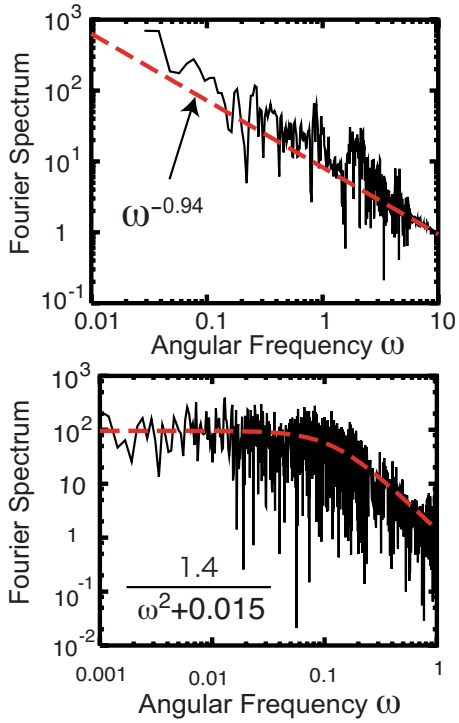

FIG. 5. (Color online) Fourier spectra (solid lines) of the time correlation of the action J_1 (a) for a trajectory of the power law decay, and (b) for a trajectory of the exponential decay (solid lines). Fittings by $1/\omega$ and $a/(\omega^2+b)$ are shown by dashed lines.

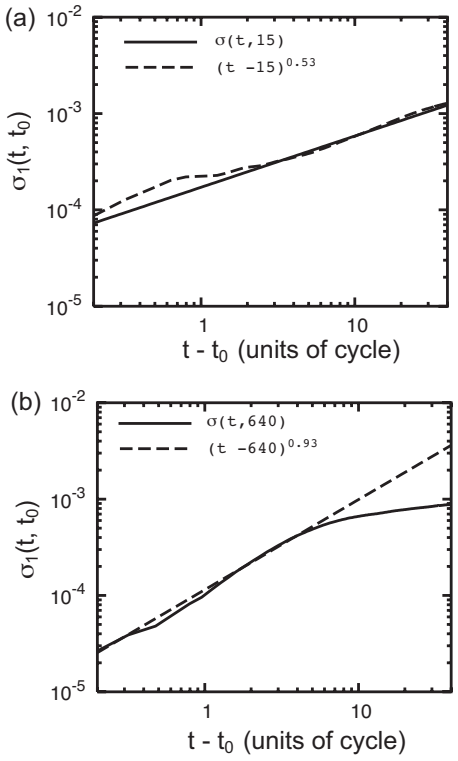

FIG. 6. Diffusivity in the action space $\sigma_1(t,t_0)$ shown as a log-log plot (solid lines) (a) for the trajectories with residence times $90<t_r<100$ with $t_0=15$, and (b) for the trajectories with residence times $1500<t_r<2000$ with $t_0=640$. The fittings $(t-t_0)^p$ (dashed lines) (a) with $p=0.53$ and (b) with $p=0.93$ are also shown.

$1500<t_r<2000$. Here, we choose $t_0=640$, thereby estimating the local diffusivity in the middle of wandering within the web. Contrary to Fig. 6(a), we can see that the trajectories exhibit nearly normal diffusion, i.e., $(t-t_0)^p$ with $p=0.93$. In Fig. 6(b), the diffusivity shows saturation for later times. From the saturated value of the diffusivity $\sigma_1 \sim 10^{-3}$, we can estimate that the width of the region over which they spread is $2\sqrt{(10^{-3})} \sim 0.06$. It is about the same as the width of the region along the J_1 direction that is explored by the trajectory in Fig. 3(b). Thus, the saturation comes from the finiteness of the chaotic region in the action space.

The above results manifest the contrast in statistical features between the trajectories of the power law and of the exponential decay. The Fourier spectra of the autocorrelation and local diffusivity in the action space indicate that, while the trajectories of the exponential decay exhibit normal diffusive behavior, the trajectories of the power law decay deviate from it and exhibit subdiffusion.

VI. CONNECTION BETWEEN NHIM AND ARNOLD WEB

In this section, we study transient features of the trajectories of the exponential decay. We expect that analysis of transient behavior will reveal how these trajectories approach to (depart from) the Arnold web from (to) the NHIM near the saddle, i.e., the dynamical connection. Do they directly arrive at the resonance junctions from near the NHIM, or do they go through those regions where the distribution of resonances is sparse? The difference in approaching to (departing from) the Arnold web will be manifest in transient features of the statistical properties.

In Fig. 7, the local diffusivity $\sigma_1(t,t_0)$ for the trajectories with residence times $1500<t_r<2000$ is shown for different values of the time t_0. We have chosen the following three values for t_0; $t_0=3$, 900, and $t_r(i)-50$ where $t_r(i)$ is the residence time of the ith trajectory. These three values of t_0 correspond to times just after arriving in the Arnold web, in the middle of wandering the web, and just before departing from the web, respectively. For the three values of t_0, we obtain $(t-t_0)^p$ with $p=0.57$, 0.97, and 0.59, respectively.

In Fig. 8, the power p in $(t-t_0)^p$ is shown as a function of the time t_0. The values of p are near 0.5 when the trajectories are those just after arriving at the Arnold web, and just before leaving it. On the other hand, the values of p are near 1.0 in between these two time regions. Thus, the system exhibits subdiffusion just after arriving at the Arnold web and just before leaving it. On the contrary, they show normal diffusion in the middle of the period of wandering the web.

In Fig. 9, the windowed Fourier spectra of the autocorrelation of J_1 exhibit corresponding statistical features. There, the results for a typical example of the trajectories of the exponential decay are shown. Other examples of the trajectories of exponential decay exhibit the same features. We have chosen four time windows, i.e., Fig. 9(a), just after arriving at the web, Figs. 9(b) and 9(c), in the middle of wandering the web, and Fig. 9(d), just before departing the

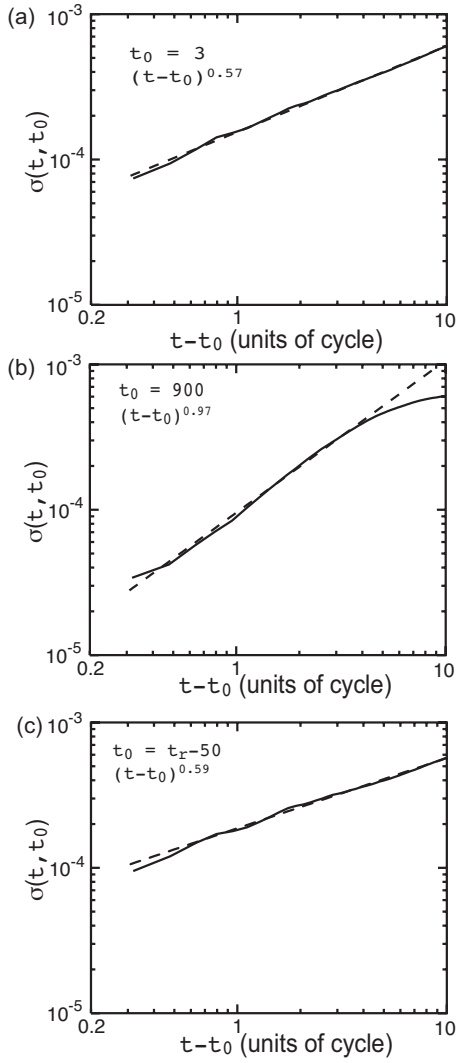

FIG. 7. Local diffusivity $\sigma_1(t,t_0)$ for the trajectories with residence times $1500<t_r<2000$ shown by log-log plots (solid lines) with fittings $(t-t_0)^p$ (dashed lines). Different values of the time t_0 are chosen as t_0=(a) 3, (b) 900, and (c) $t_r(i)-50$, where $t_r(i)$ is the residence time of the ith trajectory.

web. These four windows are indicated in Fig. 9(e) with the corresponding statistical features. The windowed Fourier spectra exhibit the changes $1/f \rightarrow$ Lorentzian $\rightarrow 1/f$. These changes correspond to the changes shown by the local diffusivity in Fig. 8.

These results indicate that the trajectories of the exponential decay first arrive in the remote regions from the resonance junctions, thereby exhibiting subdiffusion. After spending some time there, they migrate into regions near the resonance junctions, showing normal diffusion. When they leave the web, they migrate again to regions remote from the junctions, and exit the well. These trajectories spend most of their time near the resonance junctions. Therefore, the dynamics there determine their statistical features. Thus, analysis of the transient features of the statistical properties reveals the dynamical connection between the NHIM around the saddle and the Arnold web.

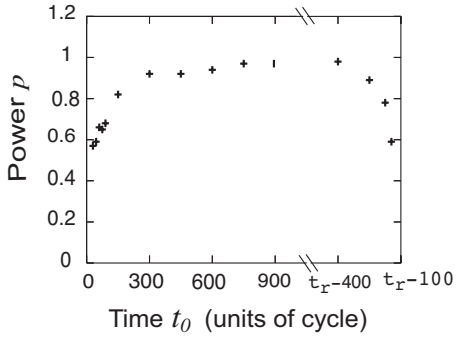

FIG. 8. Power p in the fitting $(t-t_0)^p$ as a function of the time t_0 for the trajectories with residence times $1500<t_r<2000$, i.e., exponential decay.

We also note that, contrary to the Fourier spectrum in Fig. 5(b), the windowed Fourier spectra in Figs. 9(b) and 9(c) exhibit pronounced peaks with several higher harmonics above the Lorentzian background. This indicates that the action J_1 temporarily exhibits oscillatory motions while the trajectory is wandering in the web. The existence of these peaks means that effects of certain resonances are enhanced in these time intervals. The magnitudes of these effects vary as the trajectory wanders in the well. Thus, their variations reveal transient features of the effects of these resonances. This will be further explored in Sec. VII using wavelet analysis.

VII. WAVELET ANALYSIS OF RESONANT BEHAVIOR

A. Time-frequency analysis based on wavelet

In this section, we perform a time-frequency analysis using wavelets to investigate transient features of resonances. The time-frequency analysis based on wavelets enables us to extract the effects of resonances including higher-order ones [41–43]. Thus, this will reveal how the trajectory experiences the effects of different resonances as it is wandering around in the Arnold web. By comparing these variations to the location of the trajectory in the web, we can identify where the effects of the resonances are enhanced.

The wavelet is regarded as a windowed Fourier transformation where the widths of the windows are adjusted according to the frequencies. For a given time series $f(t)$, the wavelet transformation $\hat{f}(\omega,t)$ is defined as

$$\hat{f}(\omega,t) = \sqrt{\frac{\omega}{\delta}}\left(\frac{2}{\pi}\right)^{1/4}\int_{-\infty}^{\infty} ds \times f(s)\exp[-i\omega(s-t)-\omega^2(s-t)^2/\delta^2], \quad (10)$$

where t is the time and ω plays the role of the frequency in the time region around t. The parameter δ determines the width of the windows. If the value of δ is too small, we have difficulty in precisely assigning the frequencies. If it is too large, the information concerning the transient features will be lost. We have found that the value $\delta=10$ is suitable for extracting the resonance structures. This is a continuous wavelet transformation and is called the Morlet wavelet.

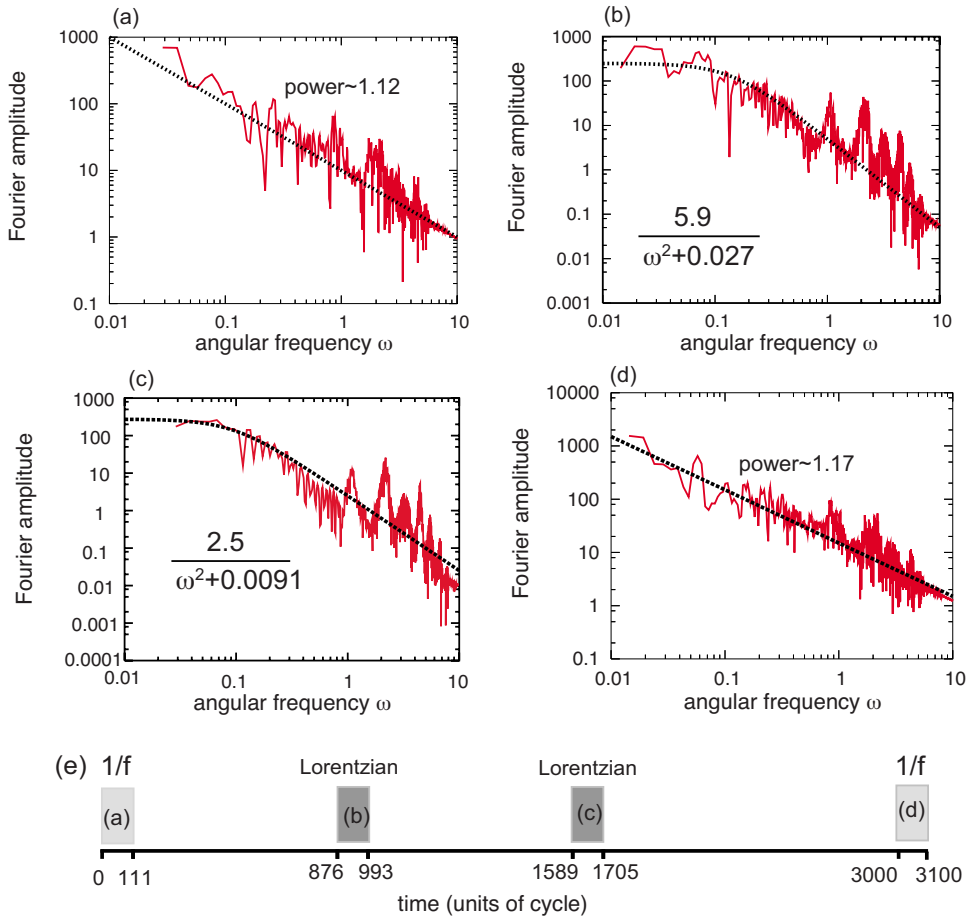

FIG. 9. (Color online) Windowed Fourier spectra of the autocorrelation of the action J_1 for a typical trajectory of the exponential decay. Four time windows are chosen: (a) just after arriving at the web, (b) and (c) in the middle of wandering the web, and (d) just before departing the web. These four windows are indicated in (e) with the corresponding statistical features.

Note that the spectrogram $S(\omega,t)=|\hat{f}(\omega,t)|^2$ gives the energy density around the frequency ω at time t.

To study resonances, we extract the ridges of the spectrogram, i.e., local maxima of $S(\omega,t)$, as a function of ω at a given value of t [42]. The ridges are regarded as those frequency regions where the energy of the time series concentrates. By extracting the ridges, we can estimate how the values of the frequencies of the time series vary. For given multiple time series $f_i(t)$ $(i=1,2,\ldots)$, we compare the values of the ridges $\omega_i(t)$ $(i=1,2,\ldots)$ to see if the ratios of these values $\omega_i(t)/\omega_j(t)$ $(i\neq j)$ are rational numbers. If the ratios are near to rational numbers with relatively simple denominators, the time series $f_i(t)$ and $f_j(t)$ are considered to be in resonance in the time interval around t.

In applying the above procedures, we use the time series of the coordinates $q_i(t)$ $(i=1,2,3)$. We estimate the values of the ridges from the highest to the nth highest ones. For a time series $q_i(t)$, we denote its kth highest ridge by $\omega_i^{(k)}(t)$ with $1\leqslant k\leqslant n$. We calculate the ratios $\omega_i^{(k)}(t)/\omega_j^{(l)}(t)$ $(i\neq j)$ to see if they satisfy resonance conditions.

In Fig. 10, we show a typical example of resonances. Here, we plot the time development of the ridges $\omega_i^{(k)}(t)$ $(1\leqslant k\leqslant 4)$ of the coordinates (a) $q_1(t)$ and (b) $q_2(t)$, for a trajectory of the exponential decay. We can see that the ratios $\omega_2^{(k)}(t)/\omega_1^{(l)}(t)$ are approximately equal to rational numbers such as 1, 2, 1/2, 4, and 1/4, although the oscillatory behavior of the frequencies causes slight deviations from the exact equality. Moreover, the oscillatory behaviors of the frequencies with approximately equal values are almost in phase between the coordinates $q_1(t)$ and $q_2(t)$. This indicates that energy exchange due to resonances takes place between the two coordinates, resulting in oscillatory variations of the frequencies. These oscillatory variations of the frequencies give rise to the peaks of the windowed Fourier spectra of the action J_1 observed in Figs. 9(b) and 9(c).

B. Arnold web with higher-order resonances

In order to visualize these resonances, we plot the ratios of the frequencies in the plane where the abscissa is $\omega_2^{(k)}(t)/\omega_1^{(l)}(t)$ and the ordinate is $\omega_3^{(m)}(t)/\omega_1^{(l)}(t)$. This is another representation of the Arnold web.

We use the highest and the second-highest ridges, i.e., $k=1,2$, $l=1,2$, and $m=1,2$. Among various combinations of the ratios $[\omega_2^{(k)}(t)/\omega_1^{(l)}(t),\omega_3^{(m)}(t)/\omega_1^{(l)}(t)]$, we expect that the larger the intensities of the ridges, the more they affect the statistical properties. Thus, we order these combinations according to the geometric mean of the intensities of the ridges $s_1^{(l)}(t)s_2^{(k)}(t)s_3^{(m)}(t)$, where $s_i^{(k)}(t)$ indicates the intensity of the kth ridge for the ith degree of freedom. We break them down into two classes, i.e., those with larger mean intensities and those with smaller ones, and show those combinations with larger mean intensities. In the following, we simply write ω_1 instead of $\omega_1^{(l)}(t)$ and so on.

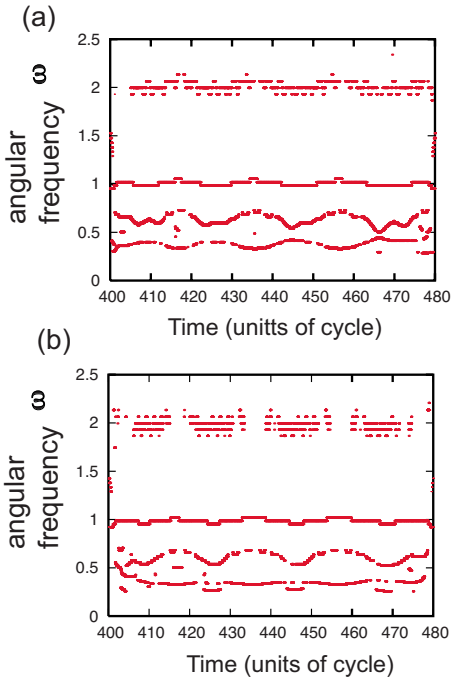

FIG. 10. (Color online) Plots of the ridges from the highest to the fourth-highest ones of the coordinates of (a) $q_1(t)$ and (b) $q_2(t)$, for a trajectory of exponential decay. The ratios $\omega_2^{(k)}(t)/\omega_1^{(l)}(t)$ attain rational numbers, indicating resonant behavior.

In Fig. 11(a), we plot the ratios of the frequencies for a trajectory of the power law decay. Other trajectories of the power law decay exhibit similar features. In Fig. 11(b), we draw some of the resonance lines identified in Fig. 11(a). For example, we can recognize the resonances $\omega_2/\omega_1=a$ with a approximately equal to 1/3, 1/2, 3/4, 1, 3/2, 2, and 3, the resonances $\omega_3/\omega_1=b$ with b approximately equal to 3/4 and 3/2, and the resonances $\omega_3/\omega_2=c$ with c approximately equal to 1/4, 1/2, 3/5, 1, 2, and 3, although their values estimated in the plots sometimes deviate slightly from the exact equality. These deviations are caused by the oscillatory behavior of the frequencies, as pointed out when we discussed the results shown in Fig. 10. These resonances are summarized in Table I.

Moreover, these plots tend to be distributed around the intersections of these lines and do not spread along the resonance lines. This reveals the effects of the resonance junctions involving higher-order resonances, and these resonance junctions do not overlap with each other.

We display in Fig. 11(c) the trajectory in the action space. It wanders away from the junctions of the primary resonances as in Fig. 3(a). In these regions, there exist rich resonance structures created by the junctions of high-order resonances as shown in Fig. 11(b). Thus, we suggest that the resonance junctions involving high-order resonances play an important role for understanding the statistical features of the trajectories of the power law decay.

In Fig. 12, temporal features of the ratios of the frequencies $(\omega_2/\omega_1, \omega_3/\omega_1)$ are plotted for a trajectory of the exponential decay with the residence time $t_r=800$. Here, we choose the following four time intervals: $t=$ (a) 0–80, (b) 400–480, (c) 560–640, and (d) 720–800; (a) is just after arriving in the web, (b) and (c) are in the middle of wandering the web, and (d) is just before departing from the web. In Figs. 13(a) and 13(b), we draw the resonance lines for Figs. 12(a) and 12(b), respectively. These resonances are summarized in Tables II and III, respectively.

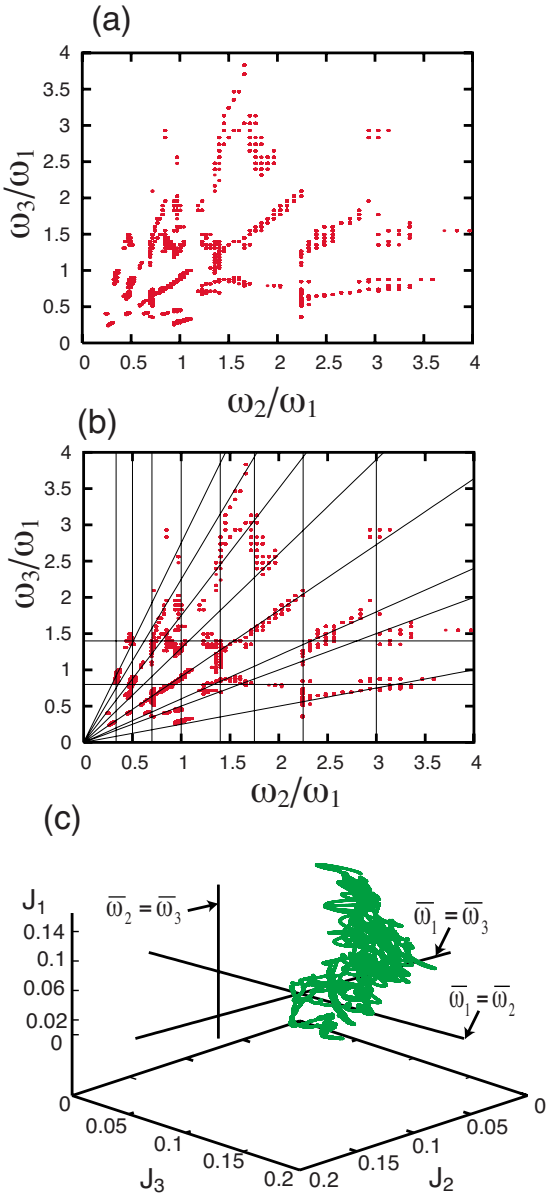

FIG. 11. (Color online) (a) Resonance structures of a trajectory of power law decay with the residence time $t_r=80$ (units of cylce). (b) Resonance lines for the plots (a). (c) Corresponding trajectory in the action space.

In Figs. 12(a) and 12(d), rich structures of the junctions of higher-order resonances exist, as in Fig. 11(a). We can see that the trajectory in these time intervals is in regions remote from the junction of the primary resonances, where the junctions of high-order resonances exist. The structures have similar characteristics to that of the trajectory of the power law decay shown in Fig. 11(a). In fact, we can find common resonances in Tables I and II. Thus, we can confirm the im-

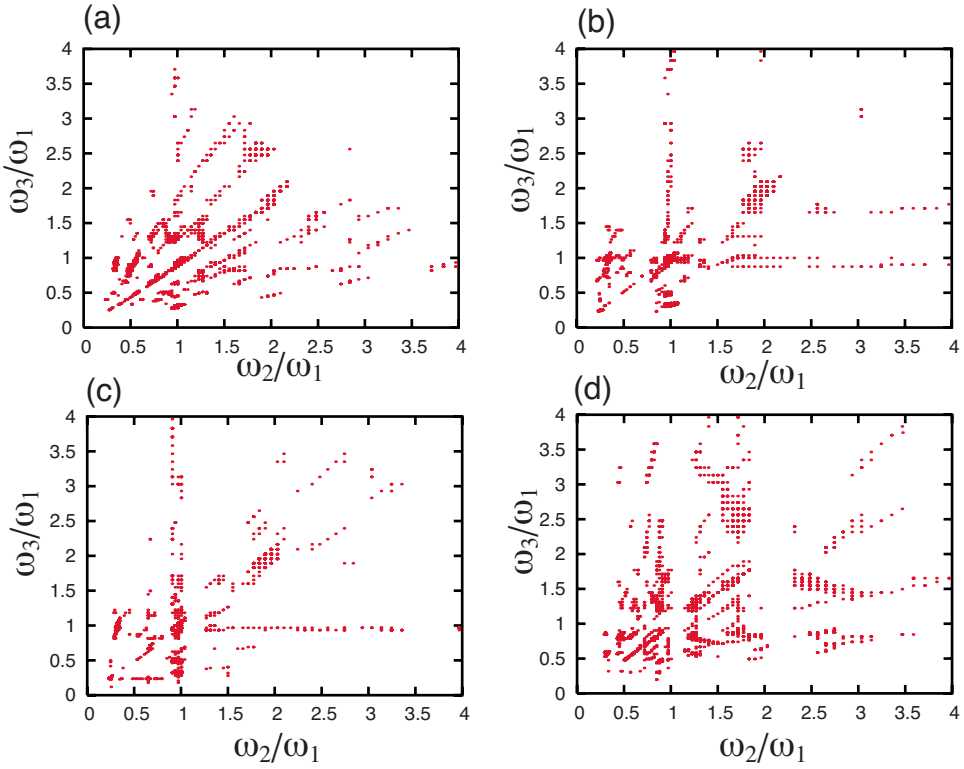

FIG. 12. (Color online) Transient resonance structures of a trajectory of exponential decay with residence time $t_r=800$ in units of the period $t_1=2\pi\omega_1$. Plots of the ratios of the frequencies are done for the following time intervals: t =(a) 0–80, (b) 400–480, (c) 560–640, and (d) 720–800.

portance of the junctions involving higher-order resonances, which play important roles in the power law decay trajectory in Fig. 11. These results also correspond to the subdiffusive behavior observed in Sec. VI.

On the other hand, in Figs. 12(b) and 12(c), the resonance line $\omega_2/\omega_1=a$ with a equal to 1 and the resonance line $\omega_3/\omega_1=b$ with b equal to 1 are especially noticeable. Moreover, some plots spread along the resonance lines $\omega_2/\omega_1=1$ and $\omega_3/\omega_1=1$, i.e., the primary resonances involving the reaction coordinate. In Fig. 12(b), the plots spread along the line $\omega_2/\omega_1=1$ for $3/2\leqslant\omega_3/\omega_1\leqslant5/2$ and along $\omega_3/\omega_1=1$ near $\omega_2/\omega_1=1/2$, 1, 2, and 3. In Fig. 12(c), the plots spread along the line $\omega_2/\omega_1=1$ near $\omega_3/\omega_1=1/2$ and $\omega_3/\omega_1=1$, and along $\omega_3/\omega_1=1$ for $3/2\leqslant\omega_2/\omega_1\leqslant5/2$. These results indicate that the junctions involving higher-order resonances overlap with each other along the primary resonances. Based on this, we suggest that the overlapping of the junctions including higher-order resonances corresponds to normal diffusion and Lorentzian spectra.

TABLE I. Resonance conditions for the power law orbit shown in Fig. 11(b).

Resonances involved	Resonance conditions
ω_2, ω_1	$\frac{\omega_2}{\omega_1}=\frac{1}{3}, \frac{1}{2}, \frac{7}{10}\left(\sim\frac{3}{4}\right), 1, \frac{7}{5}\left(\sim\frac{3}{2}\right), \frac{7}{4}(\sim2), \frac{9}{4}(\sim2), 3$
ω_3, ω_1	$\frac{\omega_3}{\omega_1}=\frac{4}{5}\left(\sim\frac{3}{4}\right), \frac{7}{5}\left(\sim\frac{3}{2}\right)$
ω_3, ω_2	$\frac{\omega_3}{\omega_2}=\frac{1}{4}, \frac{1}{2}, \frac{3}{5}, \frac{10}{11}(\sim1), \frac{13}{10}(\sim1), \frac{7}{4}(\sim2), \frac{9}{4}(\sim2), \frac{11}{4}(\sim3)$

C. Similarity of resonance structures

Thus, the distribution of those combinations of the frequencies with stronger mean intensities exhibits clear correspondence with the difference of the statistical properties. On the other hand, those with smaller mean intensities do not show such tendencies. This justifies our procedure of dividing the combinations of the frequencies according to their mean intensities. This is crucial for studying the origin of the difference in the statistical properties. Note that the pattern recognition and quantification of the resonance structures, to determine that the system locally has two distinct dynamical

TABLE II. Resonance conditions for the exponential decay shown in Fig. 13(a).

Resonances involved	Resonance conditions
ω_2, ω_1	$\frac{\omega_2}{\omega_1}=\frac{1}{3}, \frac{3}{4}, 1, \frac{5}{4}\left(\sim\frac{4}{3}\right), \frac{7}{4}(\sim2), \frac{5}{2}$
ω_3, ω_1	$\frac{\omega_3}{\omega_1}=\frac{1}{3}, \frac{1}{2}, \frac{4}{5}\left(\sim\frac{3}{4}\right), \frac{7}{5}\left(\sim\frac{3}{2}\right), \frac{5}{2}$
ω_3, ω_2	$\frac{\omega_3}{\omega_2}=\frac{1}{4}, \frac{2}{5}, \frac{1}{2}, \frac{2}{3}, \frac{10}{11}(\sim1), \frac{5}{4}\left(\sim\frac{4}{3}\right), \frac{7}{5}\left(\sim\frac{3}{2}\right), \frac{7}{4}(\sim2), \frac{11}{4}(\sim3)$

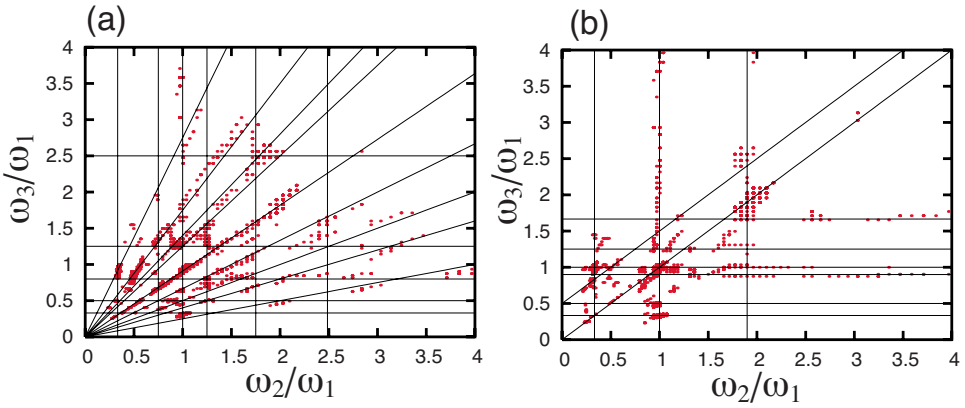

FIG. 13. (Color online) Resonance lines for the plots shown in Fig. 12. (a) is for Fig. 12(a) and 12(b) is for Fig. 12(b).

regimes, i.e., exponential and power law decays, is not a trivial task at all. Indeed, we found that the frequency combinations, irrespective of the intensity, cannot straightforwardly differentiate the resonance structures that appeared in the frequency ratio space (however, this may not necessarily mean that one can ignore any low-intensity frequency ratio).

We also recognize that the transient features of the resonances are similar between Figs. 12(b) and 12(c). To estimate the similarity of the resonance structures quantitatively, we calculate the distance of the distributions of resonances using the Hellinger distance d_H [44]:

$$d_H(f,g) = \left(\int [\sqrt{f(x)} - \sqrt{g(x)}]^2 dx \right)^{1/2},$$

where $f(x)$ and $g(x)$ are normalized distributions of the N-dimensional quantity x. The results are shown in Fig. 14. We can confirm that the distance between the distributions of the resonances for (b) and (c) is the smallest. This indicates that the trajectory experiences similar resonance structures while it wanders around the junctions of the primary resonances. This is because resonance overlap destroys fine structures of higher-order resonances and replaces them by the local ergodic component shown in Fig. 3. On the other hand, the distance between (a) and (d) takes a lager value. This means that variety of resonance structures exists in the entrance (a) and exit (d) regions since various combinations of higher-order resonances are possible. Thus, the pattern recognition and estimate of the distances between the transient resonance structures offer new approaches to differentiating the statistical properties of trajectories from the dynamical viewpoint.

Note the following points. The features we have seen in this section, i.e., the similarity in the resonance structures of the power law decay trajectory [Fig. 11(a)] and the entrance and the exit parts of the exponential decay trajectory [Figs. 12(a) and 12(d)], and the simplicity of the resonance structures of the middle parts of the exponential decay trajectory [Figs. 12(b) and 12(c)] compared to the entrance and exit parts [Figs. 12(a) and 12(d)], can be observed in other trajectories. Moreover, they confirm the transient properties obtained by the statistical investigation in the previous section. Therefore, the results obtained in this section based on a few trajectories are not restricted to a specific trajectory but are applicable to the whole system.

TABLE III. Resonance conditions for the exponential decay shown in Fig. 13(b).

Resonances involved	Resonance conditions
ω_2, ω_1	$\frac{\omega_2}{\omega_1} = \frac{1}{3}, 1, \frac{19}{10}(\sim 2)$
ω_3, ω_1	$\frac{\omega_3}{\omega_1} = \frac{1}{3}, \frac{1}{2}, \frac{9}{10}(\sim 1), 1, \frac{5}{4}\left(\sim\frac{4}{3}\right), \frac{5}{3}$
ω_3, ω_2	$\frac{\omega_3}{\omega_2} = 1$
ω_1, ω_2, ω_3	$2\omega_3 = 2\omega_2 + \omega_1$

D. Summary

In this section, we have studied the temporal variance of the resonant behavior using wavelet analysis. The wavelet analysis has enabled us to extract resonant behavior including higher-order resonances. We suggest that the characteristics of the resonance junctions including higher-order resonances play an important role for understanding the statistical features of the trajectories. In particular, nonoverlapping of the junctions of higher-order resonances causes the fractional behavior. On the other hand, overlapping of these junctions results in normal statistical behavior. Thus,

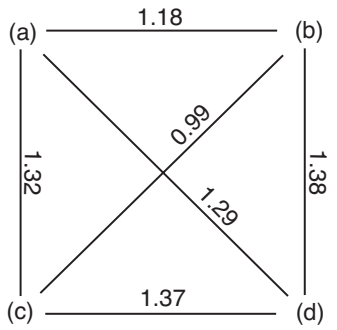

FIG. 14. Hellinger distance between the distributions in Fig. 12.

the difference of the distributions of the resonance junctions explains the coexistence of the power law and exponential decays. In a future presentation we will refine the results for transient resonance structures by incorporating other methods such as the fast Lyapunov indicator [45]. This will improve the accuracy in identifying resonances including resonance junctions.

VIII. ROBUSTNESS OF FRACTIONAL BEHAVIOR

In this section, we show that the coexistence of the power law and exponential decays persists as we change the energy or the parameters of the Hamiltonian.

In Fig. 15, the survival probabilities are shown for different values of the energy. The graph for $E=0.1$ is the same as the one shown in Fig. 2. We note that the coexistence of the power law and exponential decays persists as we change the energy. The values of the exponent α of $\exp(-\alpha t_r)$ vary considerably, however. On the contrary, the values of the power γ of $t_r^{-\gamma}$ do not change, as is shown in Fig. 15(c). This suggests that the mechanism which determines the power in the fractional behavior is more robust compared to the mechanism determining the exponents in the exponential decay.

In Fig. 16, the survival probabilities are shown as we change the strength of the coupling terms in Eq. (3). Here, we change the value of the parameter a_2 in the coupling terms between the reaction coordinate and the bath coordinates. By changing the value of a_2, we can vary the energy exchange between the reaction coordinate and the bath coordinates, causing a large variance in the survival probability. The energy is set to be $E=0.1$ here.

In Fig. 16(a), the coexistence of the power law and exponential decays persists as we change the values of the parameter between $a_2=0.9$ and 1.5. However, as we weaken the coupling a_2 further from $a_2=0.9$, the exponential decay around $t_r=1000$ is replaced by power law decay. Moreover, in Fig. 16(b), the exponents of the exponential decay for $t_r \geqslant 2000$ show a large difference between $a_2=0.9$ and 0.8. This suggests that a transition takes place in geometric structures of the phase space between $a_2=0.9$ and 0.8. We can think of two possibilities for the mechanism of the transition: One is related to the Arnold web, and the other to the connection between the NHIM and the web. The first possibility is the following. For larger values of the coupling, the resonance junctions overlap, including the junctions involving higher-order resonances. As we weaken the coupling, the widths of the resonances shrink so that these resonance junctions start to be separated from each other. Thus, the junctions involving the reaction coordinate no longer overlap, thereby replacing the exponential decay by power law decay. The second possibility is the following. As we weaken the coupling term, the energy exchange becomes weaker between the reaction coordinate and the bath coordinates. This makes the dynamical connection between the NHIM around the saddle and the Arnold web narrower. Detailed studies for these possibilities will be done in a future presentation.

In this section, we have shown that the coexistence of the power law and exponential decays in the survival probability persists as we change the energy or the strength of the coupling term. We have also suggested that a transition of the geometric structure exists in the Arnold web and/or the dynamical connection between the NHIM and the web as we change the coupling term between the reaction coordinate and the bath coordinates.

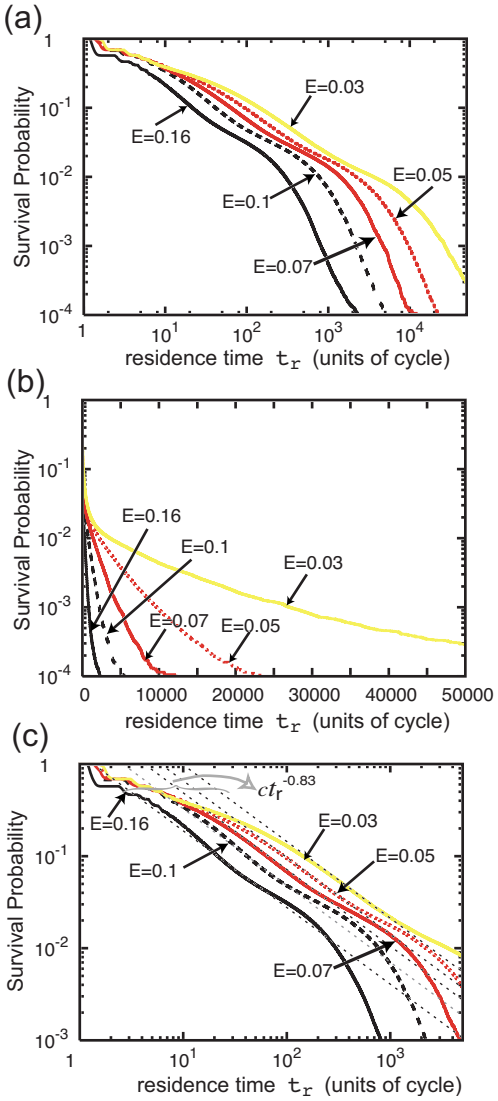

FIG. 15. (Color online) Survival probability with $E=0.16$, 0.1, 0.07, 0.05, and 0.03 as a function of the residence time t_r shown by (a) log-log plots and (b) log-linear plots. (c) Fitting of the survival probability using the power law decays $t_r^{-0.83}$.

IX. CONCLUSION AND FUTURE PROBLEMS

In this paper, we have presented numerical evidence of the fractional behavior for nonergodic reaction processes. The fractional behavior is characterized by power law decay in the survival probability, $1/f$ behavior of the Fourier spectra, and subdiffusion in the action space. We have also shown that the transient features of these quantities reveal the dynamical connection between the NHIM around the saddle and the Arnold web, i.e., how the trajectories on the unstable manifold of the NHIM arrive in the Arnold web, wander

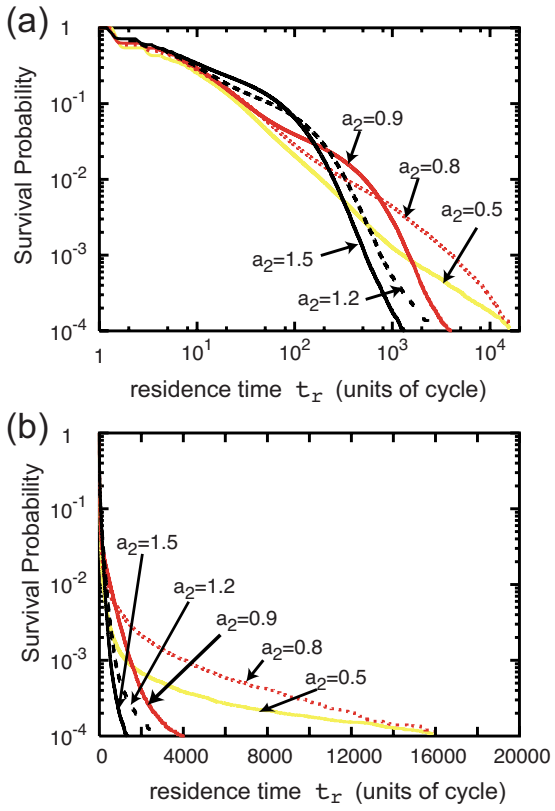

FIG. 16. (Color online) Survival probability with $a_2=1.5$, 1.2, 0.9, 0.8, and 0.5 for the energy $E=0.1$ as a function of the residence time t_r shown by (a) log-log plots and (b) log-linear plots.

around, and depart from it. In particular, a wavelet analysis reveals transient features of the resonant behavior including higher-order resonances. Based on the results of the wavelet analysis, we present the following conjectures. While nonoverlapping of the junctions of higher-order resonances corresponds to fractional behavior, overlapping of these junctions reduces the hierarchical structures, thereby giving rise to normal diffusive behavior. Thus, the characteristics of the resonance junctions including higher-order ones play an important role in understanding the statistical features. We have also shown that the coexistence of the power law and exponential decays in the survival probability persists as we change the energy or the strength of the coupling term.

Recently, the coexistence of power law and exponential decays in the survival probability was also found for a Hamiltonian of real reaction processes [46]. Note that existence of fractional behavior casts doubt on the definability of the rate constant in the phenomenological description of reactions. Thus, the limitation of the definability of the rate constant should be taken into account for nonergodic processes in real molecular systems. Moreover, fractional behavior in reactions opens the possibility of Maxwell's demon in molecular systems [47]. Therefore, the existence of the fractional behavior is important in considering the mechanism of information processing at the molecular level.

At the molecular level, the fractional behavior in IVR has been investigated in quantum [8,9,15] and classical systems [16,48]. One of the possible models to analyze these results is the local random matrix model [49]. However, the model does not take into account the geometric structure of phase space. In particular, the connection between the NHIM around the saddle and the Arnold web is beyond the present random matrix model. We think that not only the hierarchical structures in the web, but also their connection, must play an important role in determining the power in the fractional behavior. Therefore, we need to develop a method to bridge the gap between the geometric structures of phase space and phenomenological random matrix models.

The dynamical origins of the fractional behavior in multidimensional Hamiltonian systems is an open problem in the field of nonlinear science. The hierarchical ordering of POs for multidimensional Hamiltonian systems is revealed in a recent study [30]. The authors argue that the hierarchical ordering corresponds to hierarchical structures of resonant tori in the integrable limit of the Hamiltonian. On the other hand, resonance junctions constitute a hierarchical structure characterized by the Hasse diagram [36]. Therefore, we need to investigate whether these hierarchical structures explain the existence of the fractional behavior in multidimensional Hamiltonian systems.

Moreover, for the fractional behavior in reactions, intersections between the unstable and stable manifolds of these hierarchical structures and those of the NHIM around the saddle play an important role. There exists a study which investigates unstable POs in the resonance junctions [29]. However, the dimensions of the stable (unstable) manifolds of each PO are too small to contribute to the reaction processes. Instead of individual POs, the hierarchical set of POs constitutes a larger-dimensional structure in the phase space. Therefore, the intersection of its stable (unstable) manifolds with those of the NHIM around the saddle gives a more significant contribution to reactions. Whiskered tori in the resonance junctions have also been studied [26–28]. They offer another mechanism for the fractional behavior, if they constitute a hierarchical ordering. Then, the hierarchical set of whiskered tori gives larger dimensional intersections, contributing more significant effects for the reactions.

We also need to investigate quantum effects that correspond to fractional behavior in reactions. It is shown that the fractional behavior corresponds for classical and quantum systems for low-dimensional maps [50]. It is also known that the larger the number of degrees of freedom, the more likely the correspondence holds [51]. Thus, we expect that the fractional behavior plays a crucial role in the dynamics of reaction processes in multidimensional Hamiltonian systems. These subjects will be studied elsewhere.

ACKNOWLEDGMENTS

A.S. would like to acknowledge the referees for their fruitful comments. This work is supported by JSPS, Grant-in-Aid for Research on Priority Area "Control of Molecules in Intense Laser Fields," MEXT, JST/CREST, 21st century COE (Center Of Excellence) of "Origin and Evolution of Planetary Systems (Kobe University)," MEXT, and a Discretionary Research Grant of the University President for Researchers of Nara Women's University.

[1] G. M. Zaslavsky, *Hamiltonian Chaos and Fractional Dynamics* (Oxford University Press, Oxford, 2004).
[2] Y. Y. Yamaguchi, Int. J. Bifurcation Chaos Appl. Sci. Eng. **7**, 839 (1997).
[3] A. Baba, Y. Hirata, S. Saito, and I. Ohmine, J. Chem. Phys. **106**, 3329 (1997).
[4] A. Shudo and S. Saito, Adv. Chem. Phys. **130B**, 375 (2005).
[5] J. Barre, F. Bouchet, T. Dauxois, S. Ruffo, and Y. Y. Yamaguchi, Physica A **365**, 177 (2006).
[6] Y. Y. Yamaguchi, F. Bouchet, and T. Dauxois, J. Stat. Mech.: Theory Exp. 2007, P01020.
[7] R. D. Levine, *Molecular Reaction Dynamics* (Cambridge University Press, Cambridge, U.K., 2005).
[8] V. Wong and M. Gruebele, J. Phys. Chem. A **103**, 10083 (1999).
[9] M. Gruebele, J. Phys.: Condens. Matter **16**, R1057 (2004).
[10] M. Toda, Adv. Chem. Phys. **130A**, 337 (2005).
[11] A. Shojiguchi, C.-B. Li, T. Komatsuzaki, and M. Toda, Commun. Nonlinear Sci. Numer. Simul. (to be published).
[12] A. Lichtenberg and M. Lieberman, *Regular and Chaotic Dynamics*, 2nd ed. (Springer-Verlag, Berlin, 1992).
[13] B. V. Chirikov, Phys. Rep. **52**, 263 (1979).
[14] C. Martens, M. Davis, and G. Ezra, Chem. Phys. Lett. **142**, 519 (1987).
[15] S. A. Schofield and P. G. Wolynes, Chem. Phys. Lett. **217**, 497 (1994).
[16] N. R. C. S. Keshavamurthy and S. Tomsovic, J. Chem. Phys. **117**, 4168 (2002).
[17] T. Komatsuzaki and R. S. Berry, Adv. Chem. Phys. **123**, 79 (2002).
[18] T. Uzer, C. Jaffe, J. Palacian, P. Yanguas, and S. Wiggins, Nonlinearity **15**, 957 (2002).
[19] *Geometric Structures of Phase Space in Multidimensional Chaos: Applications to Chemical Reaction Dynamics in Complex Systems*, edited by M. Toda, T. Komatsuzaki, T. Konishi, R. S. Berry, and S. A. Rice, Adv. Chem. Phys. 130A, 130B (2005), and references therein.
[20] C. B. Li, A. Shoujiguchi, M. Toda, and T. Komatsuzaki, Phys. Rev. Lett. **97**, 028302 (2006).
[21] H. Waalkens, A. Burbanks, and S. Wiggins, J. Chem. Phys. **121**, 6207 (2004).
[22] C. B. Li, Y. Matsunaga, M. Toda, and T. Komatsuzaki, J. Chem. Phys. **125**, 184301 (2005).
[23] T. Komatsuzaki and R. S. Berry, J. Chem. Phys. **110**, 9160 (1999).
[24] R. S. Berry, Adv. Chem. Phys. **130B**, 3 (2005).
[25] C. Jaffe, S. D. Ross, M. W. Lo, J. Marsden, D. Farrelly, and T. Uzer, Phys. Rev. Lett. **89**, 011101 (2002).
[26] G. Haller, Phys. Lett. A **200**, 34 (1995).
[27] G. Haller, *Chaos Near Resonance* (Springer, New York, 1999).
[28] S. Goto and K. Nozaki, Prog. Theor. Phys. **102**, 937 (1999).
[29] S. Goto, Prog. Theor. Phys. **115**, 251 (2006).
[30] S. Gekle, J. Main, T. Bartsch, and T. Uzer, Phys. Rev. Lett. **97**, 104101 (2006).
[31] V. I. Arnold, Sov. Math. Dokl. **5**, 581 (1964).
[32] P. J. Holmes and J. E. Marsden, J. Math. Phys. **23**, 669 (1982).
[33] N. N. Nekhroschev, Usp. Mat. Nauk **32**, 6 (1977).
[34] J. Laskar, Physica D **67**, 257 (1993).
[35] S. Honjo and K. Kaneko, Adv. Chem. Phys. **130B**, 437 (2003).
[36] M. Toda, Adv. Chem. Phys. **123**, 153 (2002).
[37] P. Orlik and H. Terao, *Arrangement of Hyperplanes* (Springer, New York, 1992).
[38] N. Fenichel, Indiana Univ. Math. J. **21**, 193 (1971).
[39] N. Fenichel, Indiana Univ. Math. J. **23**, 1109 (1974).
[40] N. Fenichel, Indiana Univ. Math. J. **26**, 81 (1977).
[41] L. V. Vela-Arevalo and S. Wiggins, Int. J. Bifurcation Chaos Appl. Sci. Eng. **11**, 1359 (2001).
[42] C. Chandre, S. Wiggins, and T. Uzer, Physica D **181**, 171 (2003).
[43] A. Shojiguchi, C.-B. Li, T. Komatsuzaki, and M. Toda, Laser Phys. **17**, 1097 (2006).
[44] A. Gibbs and F. Su, Int. Statist. Rev. **70**, 419 (2002).
[45] C. Froeschlé, M. Guzzo, and E. Lega, Science **289**, 2108 (2000).
[46] A. Shojiguchi, C.-B. Li, T. Komatsuzaki, and M. Toda (unpublished).
[47] A. Shojiguchi, C.-B. Li, T. Komatsuzaki, and M. Toda, Phys. Rev. E **75**, 035204(R) (2007).
[48] A. Semparithi and S. Keshavamurthy, J. Chem. Phys. **125**, 141101 (2006).
[49] D. Leitner and P. Wolynes, Chem. Phys. Lett. **258**, 18 (1996).
[50] G. Casati, I. Guarneri, and G. Maspero, Phys. Rev. Lett. **84**, 63 (2000).
[51] M. Toda, S. Adachi, and K. Ikeda, Prog. Theor. Phys. Suppl. **98**, 323 (1989).